# Molecular model for a complete clathrin lattice from electron cryomicroscopy

**Alexander Fotin**[1], **Yifan Cheng**[2], **Piotr Sliz**[3], **Nikolaus Grigorieff**[4], **Stephen C. Harrison**[3], **Tomas Kirchhausen**[5] & **Thomas Walz**[2]

[1]*Biophysics Graduate Program,* [2]*Department of Cell Biology, Harvard Medical School, 240 Longwood Avenue, Boston, Massachusetts 02115, USA*
[3]*Department of Biological Chemistry and Molecular Pharmacology, Harvard Medical School, and Howard Hughes Medical Institute, 250 Longwood Avenue, Boston, Massachusetts 02115, USA*
[4]*Howard Hughes Medical Institute and Department of Biochemistry, Rosenstiel Basic Medical Sciences Research Center, Brandeis University, 415 South Street, Waltham, Massachusetts 02454, USA*
[5]*Department of Cell Biology and the CBR Institute for Biomedical Research, Harvard Medical School, 200 Longwood Avenue, Boston, Massachusetts 02115, USA*

.......................................................................................................................................................................................................................................................

**Clathrin-coated vesicles are important vehicles of membrane traffic in cells. We report the structure of a clathrin lattice at subnanometre resolution, obtained from electron cryomicroscopy of coats assembled *in vitro*. We trace most of the 1,675-residue clathrin heavy chain by fitting known crystal structures of two segments, and homology models of the rest, into the electron microscopy density map. We also define the position of the central helical segment of the light chain. A helical tripod, the carboxy-terminal parts of three heavy chains, projects inward from the vertex of each three-legged clathrin triskelion, linking that vertex to 'ankles' of triskelions centred two vertices away. Analysis of coats with distinct diameters shows an invariant pattern of contacts in the neighbourhood of each vertex, with more variable interactions along the extended parts of the triskelion 'legs'. These invariant local interactions appear to stabilize the lattice, allowing assembly and uncoating to be controlled by events at a few specific sites.**

Clathrin-coated vesicles carry lipids and proteins between intracellular, membrane-bound compartments[1–3]. The coat is a lattice of clathrin, which surrounds a central membrane vesicle[4]. The clathrin assembly unit is a trimer of three very extended subunits, which radiate from a central hub[5,6] (Fig. 1a). This triskelion comprises three ~190 kDa (1,675-residue) heavy chains, each bearing a single ~25 kDa light chain[5,6]. A clathrin 'leg' is about 475 Å long[7]. Its characteristic curl as seen in electron micrographs allows us to distinguish a 'proximal segment', a 'knee', a 'distal segment', an 'ankle', a 'linker' and a 'terminal domain' (Fig. 1a). Except for the terminal domain, a globular element at the amino terminus of the heavy chain, the thickness of a leg is relatively uniform. The light chains associate with the heavy-chain proximal segments[8,9], through a central segment of 71 residues with a clearly recognizable, α-helical heptad repeat[10,11].

When triskelions assemble into a coat, the legs interdigitate to create a lattice of open hexagonal and pentagonal faces. The coats exhibit a range of designs[4]. Three of the smallest, built from 28, 36 and 60 triskelions, are illustrated in Fig. 1b; we refer to them respectively as the 'mini-coat', 'hexagonal barrel' and 'soccer ball'. The hexagonal barrel or the soccer ball is probably the smallest polyhedron that can accommodate a transport vesicle.

Clathrin recruits coated-vesicle cargo through intermediary proteins known as adaptors, which determine selective inclusion of membrane anchored proteins into coated vesicles and which form an interface between the outer clathrin coat and the incorporated, cargo-bearing, membrane bilayer[1–3]. *In vitro* reconstitution of coats from purified clathrin and adaptor complexes provides relatively homogeneous specimens, with a large proportion of hexagonal barrels, suitable for study by electron cryomicroscopy[12,13]. A reconstruction at 21 Å resolution[14] showed that the legs of assembled clathrin triskelions interdigitate in the pattern illustrated in Fig. 2[15]. A triskelion hub lies at each vertex. The proximal segments radiate towards the three neighbouring vertices and project gently inward. The legs bend smoothly at the knees, and the distal segments extend towards the next vertex, where the ankles of three converging chains cross each other about 75 Å beneath the apex of the triskelion centred there. The terminal domains project towards the interior.

Two parts of the heavy chain are represented by crystal structures. The terminal domain (residues 1–330) is a seven-blade β-propeller, connected to an α-helical zigzag that forms the linker (residues 331–494)[16]. A substantial part of the proximal segment is likewise an α-helical zigzag[17]. The latter structure revealed a larger repeating motif of about 145 residues or five helical α-zigzags—the clathrin heavy-chain repeat (CHCR). Residues 543–1576 of the heavy chain
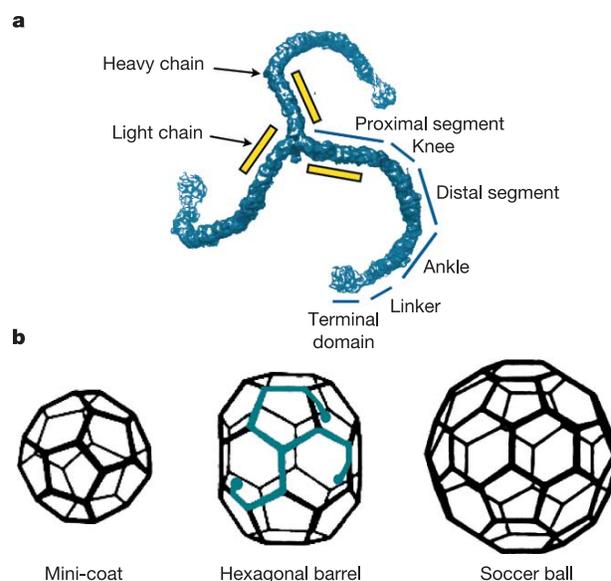
**Figure 1** The clathrin triskelion and the designs of some simple clathrin lattices.
**a**, Clathrin triskelion, labelled with names for the segments of the heavy chain. The N terminus of the chain is in the terminal domain, and the C terminus is at the vertex. Positions of the light chains are shown schematically. **b**, Three structures that form when clathrin assembles into coats *in vitro*. Mini-coats have tetrahedral symmetry; hexagonal barrels, D6 symmetry; soccer balls, icosahedral symmetry. Any surface lattice based on hexagons must have 12 pentagons to close completely. Schematic representation of one triskelion within the hexagonal barrel is shown in blue.

contain seven complete repeats, designated CHCR1–7 (ref. 17).

We have extended the resolution of clathrin hexagonal-barrel image reconstructions to subnanometre resolution (Fig. 2). We resolve a pattern of α-helical zigzags, along the complete leg, from the linker to the centre of the triskelion. The structure suggests answers to two questions that relate the molecular organization of the coat to its function in a cell. How does an assembling coat adapt to cargoes of different shapes and sizes? And how can the assembly of so elaborate a lattice be modulated by interaction with regulatory factors?
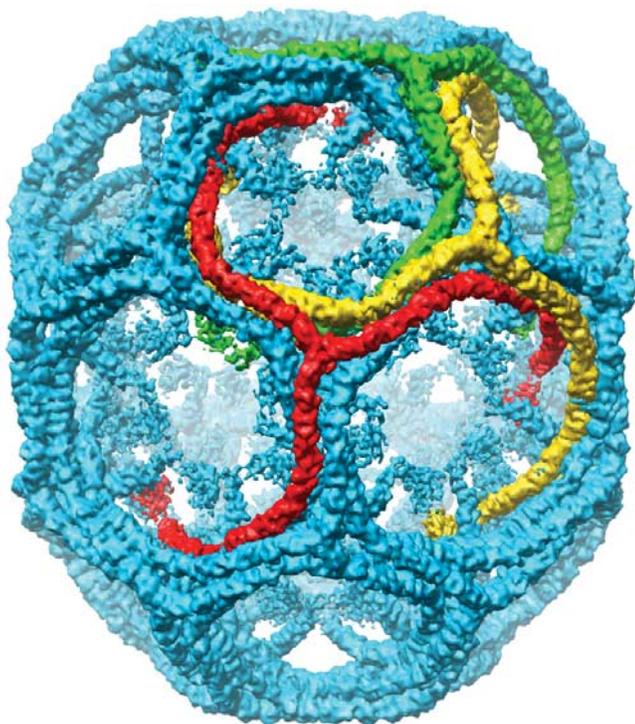
## Image reconstruction of a hexagonal-barrel coat

We reconstituted clathrin coats *in vitro* from purified bovine-brain clathrin triskelions (either intact or light-chain free) and AP-2 adaptor protein complexes (Supplementary Fig. 1a). Presence or absence of light chains did not affect the distribution of lattice designs. We selected 1,450 particles from 225 electron micrographs of light-chain-free hexagonal barrels (Supplementary Fig. 1b, c); the D6-averaged image reconstruction had a nominal resolution of 12.5 Å (using the criterion[18] that the Fourier shell correlation (FSC) = 0.143), a substantial improvement over the 21 Å resolution of the previous best structure[14]. The distribution of Euler angles for the particles (Supplementary Fig. 1d) showed that no orientations were missed. Each asymmetric unit of the barrel structure contains nine D6-symmetry independent clathrin legs[15]. By averaging corresponding segments of these legs, we could improve the signal-to-noise ratio and extend the resolution of the map. The nine independent legs align well in the proximal segment but diverge at the knee, where different degrees of bending propagate into significant changes in the positions of the distal segments and terminal domains relative to the triskelion vertex[15]. To exploit

local symmetry averaging, we split the clathrin leg into four segments, assumed to be invariant at the present resolution: proximal, distal, ankle and terminal-domain regions. We averaged the corresponding nine densities separately (see Methods). The densities of the knee regions were not averaged. The nominal resolution of the 'non-coat symmetry' (n.c.s.) averaged electron microscopy (EM) map was 7.9 Å for the proximal region (Supplementary Figs 1e and 2).

Comparison with an atomic model for residues 1280–1516 allows us to assess the reliability of the proximal-region cryoEM map (Fig. 3). The helices differ in their length and orientation, so that the model can be placed uniquely within suitably resolved densities. The averaged cryoEM density map indeed resolves individual helices in the proximal region, and we can match each helix of the atomic model with a corresponding rod-like feature of the cryoEM map (top portions in Fig. 3a–c). We can dock the atomic model as a rigid body into the cryoEM density with a correlation of 0.72. For comparison, we have computed electron density directly from the atomic model to a resolution of 7.9 Å (bottom portions in Fig. 3a–c); the calculated and observed densities are remarkably similar, confirming our assessment of the structural detail present in the EM map (see also Supplementary Fig. 2). After similar averaging of densities for the distal and ankle fragments, the nominal resolution estimates were 7.9 and 8.2 Å, respectively.

The X-ray structure of the terminal-domain-linker region[16] was used as a model for local symmetry averaging of the terminal domain densities. Our placement of the terminal domain into the cryoEM density differs from the previous fit at 21 Å resolution[15]. Rotating the terminal domain atomic model by 180° around the linker axis gives much better agreement with density. The nominal resolution of this part of the map is 11 Å, and the density is weaker than for the rest of the triskelion. The relative disorder of the terminal domains is probably a consequence of both the lack of



**Figure 2** Image reconstruction of a clathrin hexagonal barrel (heavy chains only) at 7.9 Å resolution. There are 36 clathrin triskelions in the structure, which has D6 symmetry. Thus, there are three symmetry-independent triskelions (or nine symmetry-independent legs). The coloured triskelions show one choice of the three independent triskelions. Noisy central density, from spatially disordered and substoichiometric AP-2 complexes, has been flattened.
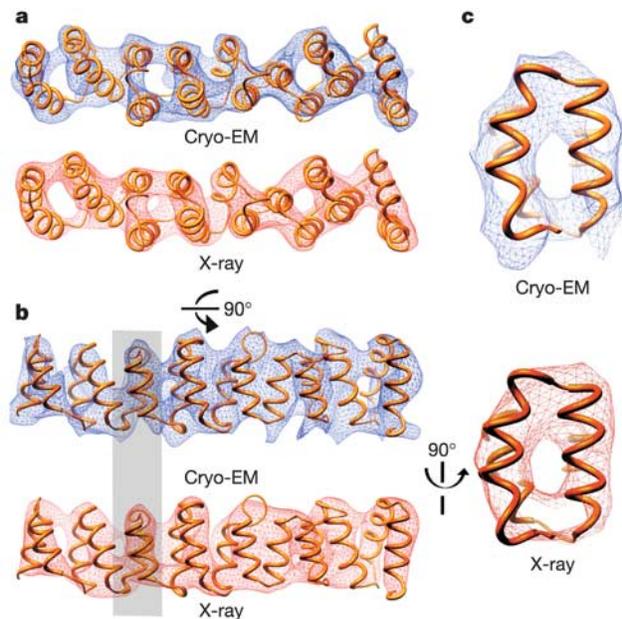


**Figure 3** Rigid-body fit of the atomic model for a segment of the proximal leg[17] to the density from the cryoEM image reconstruction. **a**, View from outside the barrel. In blue are contours of the cryoEM map; in red are contours of a map with a 7.9 Å resolution cut-off and a thermal parameter of 200, using structure factors calculated directly from the atomic model. **b**, Side view of the same. **c**, Cross-sectional view of the α-zigzag shown by the grey shading in **b**.

constraints from other contacts within the lattice and the asymmetric interactions some of them make with AP-2 complexes.

## Molecular model for a clathrin triskelion

We used sequence alignment of CHCR fragments[17] and homology modelling to derive atomic structures for the distal and ankle regions (Supplementary Fig. 3). In addition to CHCRs 1–7, we found that residues 395–542 within the linker conform well to the CHCR motif sequence profile. We designate them CHCR0.

We combined crystal structures and homology models to build atomic models for each segment of a clathrin leg. The averaged cryoEM density map had distinct structural details that allowed us to determine both translational and angular positions for each CHCR repeat within the map (Fig. 4). The docked CHCR models cover almost the entire length of a leg, without gaps or overlaps. The CHCR7 repeat extends into the trimerization region of a triskelion hub, and together with CHCR6 constitutes the proximal segment. CHCR5 forms the knee. The N terminus of CHCR5, as well as CHCRs 3 and 4, constitute the distal segment, and CHCRs 1 and 2 and the C-terminal part of CHCR0, the ankle. The helical hairpins rotate around the axis of their stack as they span a CHCR from N to C terminus, resulting in an intrinsic right-hand twist of helical

zigzags along a clathrin leg. CHCR6 in the proximal segment is rotated by roughly 90° about the leg axis relative to CHCR4 in the distal segment (Supplementary Fig. 4) and by about 180° relative to CHCR1 in the ankle (not shown).

## Helical tripod

Each vertex in the unaveraged density map has a three-fold symmetric feature projecting inwards from the top of the hub. Averaging reveals a tripod of 50-Å-long, rod-like densities (Fig. 5). The rods extend from the vertex to the crossing of two clathrin ankles, which belong to triskelions centred two vertices away. We interpret these rods as α-helices. Between them and CHCR7 is an additional 'proximal hairpin' of density. We have built residues 1577–1597 into this density as a final α-zigzag, which starts at the C terminus of CHCR7, bends around, and continues into the helix of the tripod.
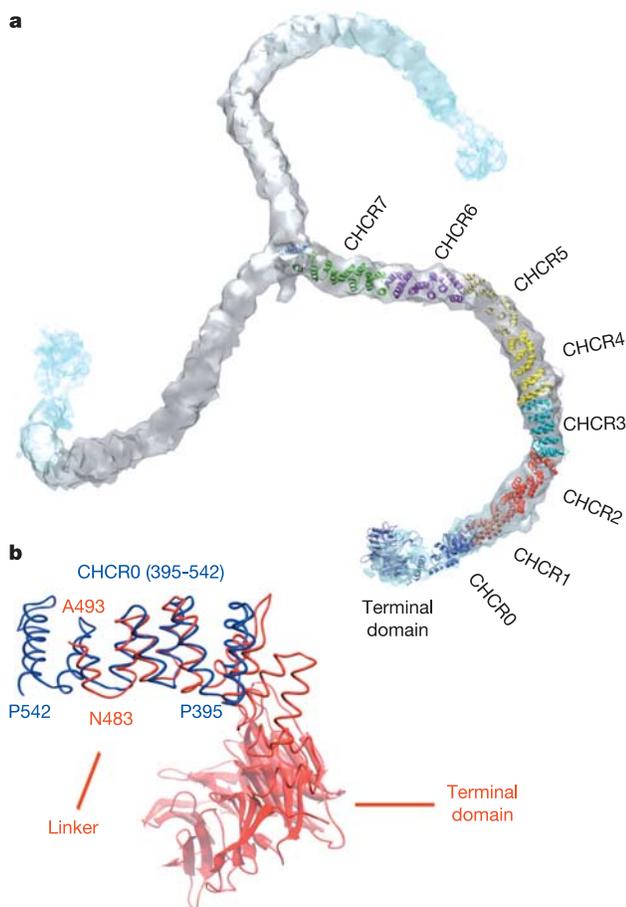


**Figure 4** Backbone model for residues 1–1597 of the clathrin heavy chain. **a**, Fit into the clathrin density of the atomic model for terminal domain and linker[16], the atomic model of CHCR6 and parts of CHCR5 and 7, and homology models of the rest of the heavy chain. For the colouring of CHCR segments and definitions of the residues at the boundaries, see Supplementary Fig. S3. **b**, Homology model for CHCR0 (blue) and the crystallographically derived model for the terminal domain and linker (red), superposed. The linker contains two additional helical hairpins, packed closely against the β-propeller terminal domain; the crystal structure lacks most of the final two hairpins of CHCR0.
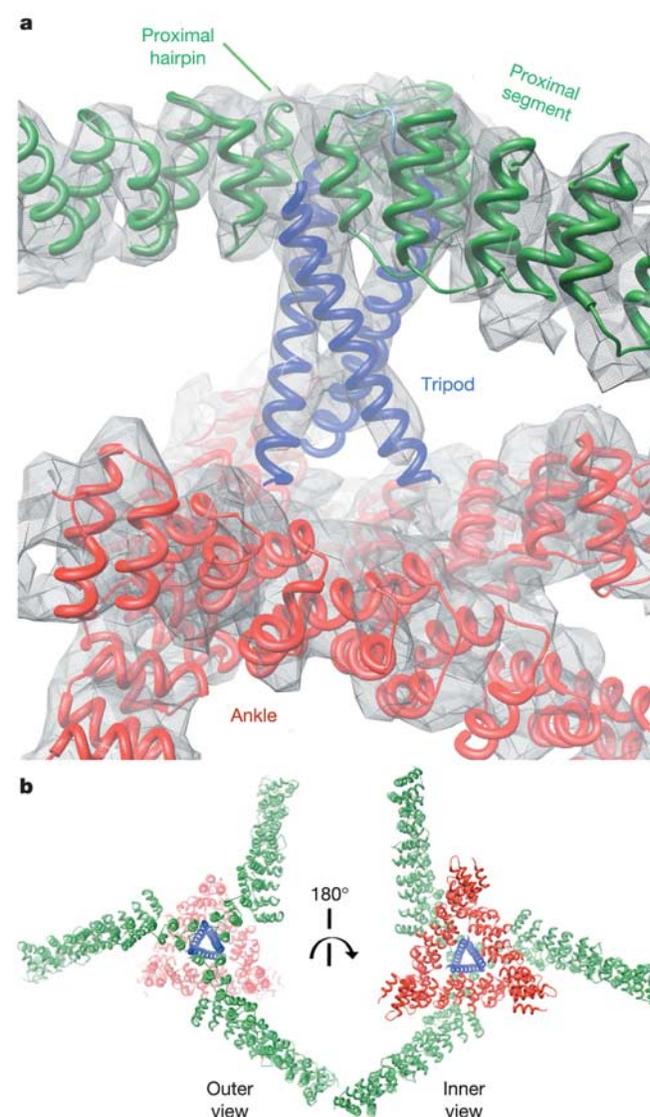


**Figure 5** The hub assembly. **a**, Fit of the heavy-chain model into density surrounding one clathrin hub. Green, the C-terminal part of CHCR7 and the proximal hairpin. Blue, the tripod helix. Red, ankle segments from triskelions centred two vertices away. The colours are those of the corresponding CHCR segment in Fig. 4a. For simplicity, the density and model corresponding to knees are not included. **b**, Views of the same region (model only) from the outside (left) and inside (right) of the barrel. Note how the tripod links the apex of the hub assembly to the braided triangle of ankles that lies about 75 Å deeper within the structure (measured from the top of the triskelion vertex).

©2004 **Nature Publishing Group**
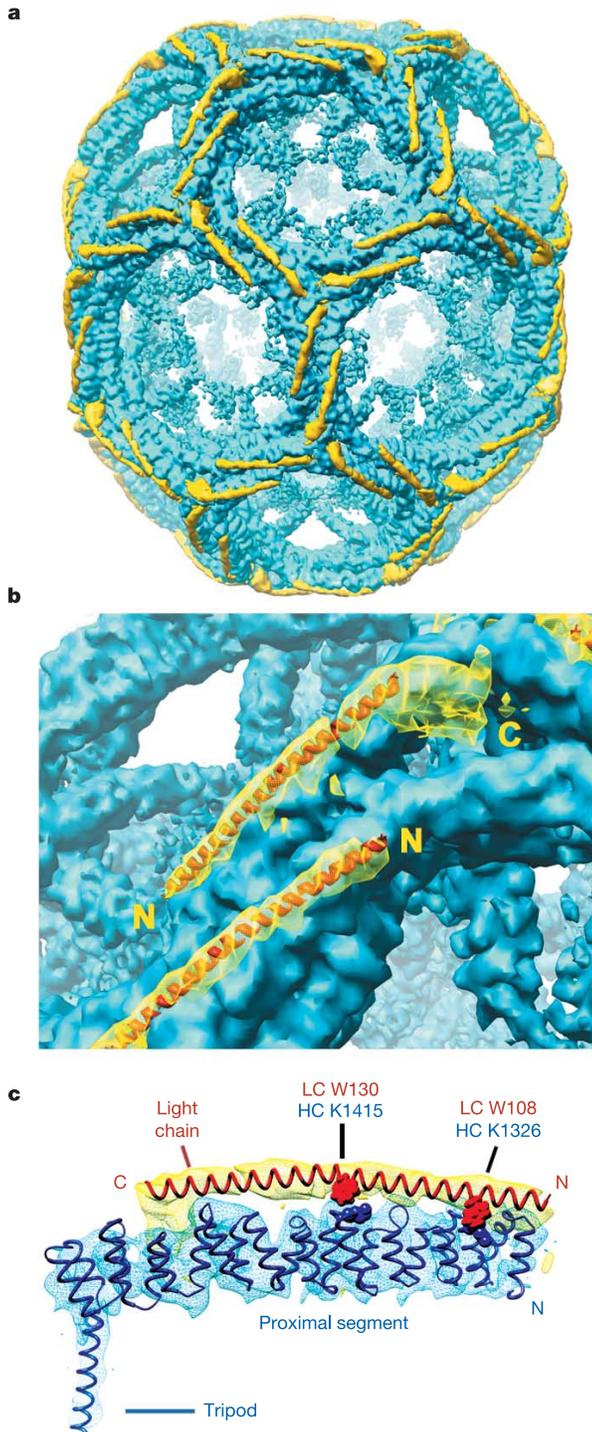
**Figure 6** Model for clathrin light chains. **a**, Differences (yellow) between the image reconstructions with and without light chains, superimposed on the light-chain-free density (blue). **b**, Close-up of the vertex to the right of centre in **a**, with a helical model for the central 71 residues of the light chain positioned in the density. A globular, but somewhat diffuse, density for the C-terminal part of the light chain reaches around the hub of the triskelion. Much weaker density (not visible here) extends inward from the N-terminal end of the long helix, perhaps representing a disordered structure for the N-terminal part of the chain. **c**, View from the side of the light-chain model (red; map contours in yellow) in relation to the α-zigzags of the heavy chain (blue). Positions of two pairs of residues, shown by compensating mutations to interact with each other[23], are marked. LC, light chain; HC, heavy chain.

The proximal hairpins from three heavy chains stack against each other to form the top of the triskelion hub. A helical model for residues 1598–1630 fits well into the rod-like density of the tripod (Fig. 5). The orientation of the helix around its axis is not determined at the resolution of the map, but its sequence (Supplementary Fig. 5) suggests an amphipathic character and reveals a conserved pattern of repeating charged residues. Residues 1598–1630 are predicted to have high helical content; there are proline residues in one or another of the aligned sequences just at the boundaries of this segment, but none within it. Clathrin heavy-chain fragments truncated at residue 1615 trimerize properly, but shorter fragments do not[19]. The tripod helices diverge, and their C-terminal ends are not in contact, precisely consistent with the biochemical observations[19].

The amino-acid sequence at the C terminus of a heavy chain (residues 1631–1675, extending beyond the tripod segment) is proline rich and varies among species more markedly than elsewhere in the clathrin heavy chain (Supplementary Fig. 5). Density potentially attributable to this final fragment merges with the ankle density, precluding definitive assignment. Our model thus includes 1,630 of the 1,675 residues in a clathrin heavy chain.

## Invariant hub

There are three symmetry independent vertices in a D6-symmetric barrel, and as none of them corresponds to an actual three-fold axis of the coat, there are nine independent ways in which the various triskelions that interdigitate beneath each vertex could make contact[15]. We find, however, that the structures in the neighbourhood of each vertex are essentially three-fold symmetric (Fig. 5), and that the three different kinds of vertices can be superimposed (not shown). In other words, the pucker of the triskelion centred at each of the vertices, the contacts between the parallel proximal and distal segments in the adjacent edges, the splay of the helical tripods, and the contacts of the tripods with the ankles beneath them are all invariant. The knees vary in the sharpness of their bend[15], but they curve gently enough to avoid the axis altogether, allowing the tripod to reach through to the ankles. The three ankle segments are braided into a triangular barrel (Fig. 5b), and the helices of the tripod terminate at the junction points of the ankle pairs, cross-linking the ankle triangle to the triskelion hub above them. The C terminus of the heavy chain may help stabilize interactions at the ankle joints, providing an 'ankle brace' to hold the entire structure together.

We describe by the phrase 'invariant hub assembly' (or, where clear from context, 'invariant hub') the tripod and three proximal segments radiating from a vertex, the distal segments (belonging to triskelions centred at nearest-neighbour vertices) lying just within those proximal segments (and running parallel to them) and the triangle of ankles (belonging to triskelions centred at second-nearest-neighbour vertices) at the foot of the tripod. We can think of the entire lattice as a set of such invariant hub assemblies, connected by more variably bent heavy-chain regions—the knees and the distal-segment-to-ankle junctions. The terminal domains and linkers hang inwards from the hub assemblies, to contact adaptors and a variety of accessory proteins.

## The light chain

We selected 1,210 particles from 240 micrographs of clathrin coats containing both heavy and light chains, produced a reconstruction at 8.2 Å resolution, and made a direct comparison with light-chain-free coats by calculating a difference map (Fig. 6). The light-chain density divides into a 100-Å-long, central, rod-like feature; a less extended and more diffuse region at the end near the vertex of the lattice; and a third, very weak feature at the other end (Fig. 6b). The polarity of the extended structure is determined by early antibody localization studies, which showed that the C-terminal part of a light chain lies near a vertex[9,20].

The rod-like density corresponds to the central, α-helical, light-chain segment, as expected, because neither the N- nor the C-terminal region is required for incorporation into a coat[21]. The length of the rod-like density corresponds precisely to an extended 71-residue α-helix, ruling out an alternative, folded model[22]. Suppressor mutagenesis studies have pinpointed two contacts (HC K1326–LCa W108 and HC K1415–LCa W130, where HC and LCa indicate heavy chain and light chain a, respectively) in the heavy-chain/light-chain interface[23]. We used this information to dock a helical model into the cryoEM density map. When one of the two pairs of interacting residues is in contact, the second pair face each other as well (Fig. 6c). We can thus determine both the translational position of the helix along the rod of density and its angular orientation about the long axis. The light-chain helix interacts with a surface formed by interhelical loops in the heavy-chain proximal segment (Fig. 6c). The axis of the light chain, which tilts relative to the axis of the heavy chain, roughly follows the right-hand twist of the heavy-chain α-helical zigzags.
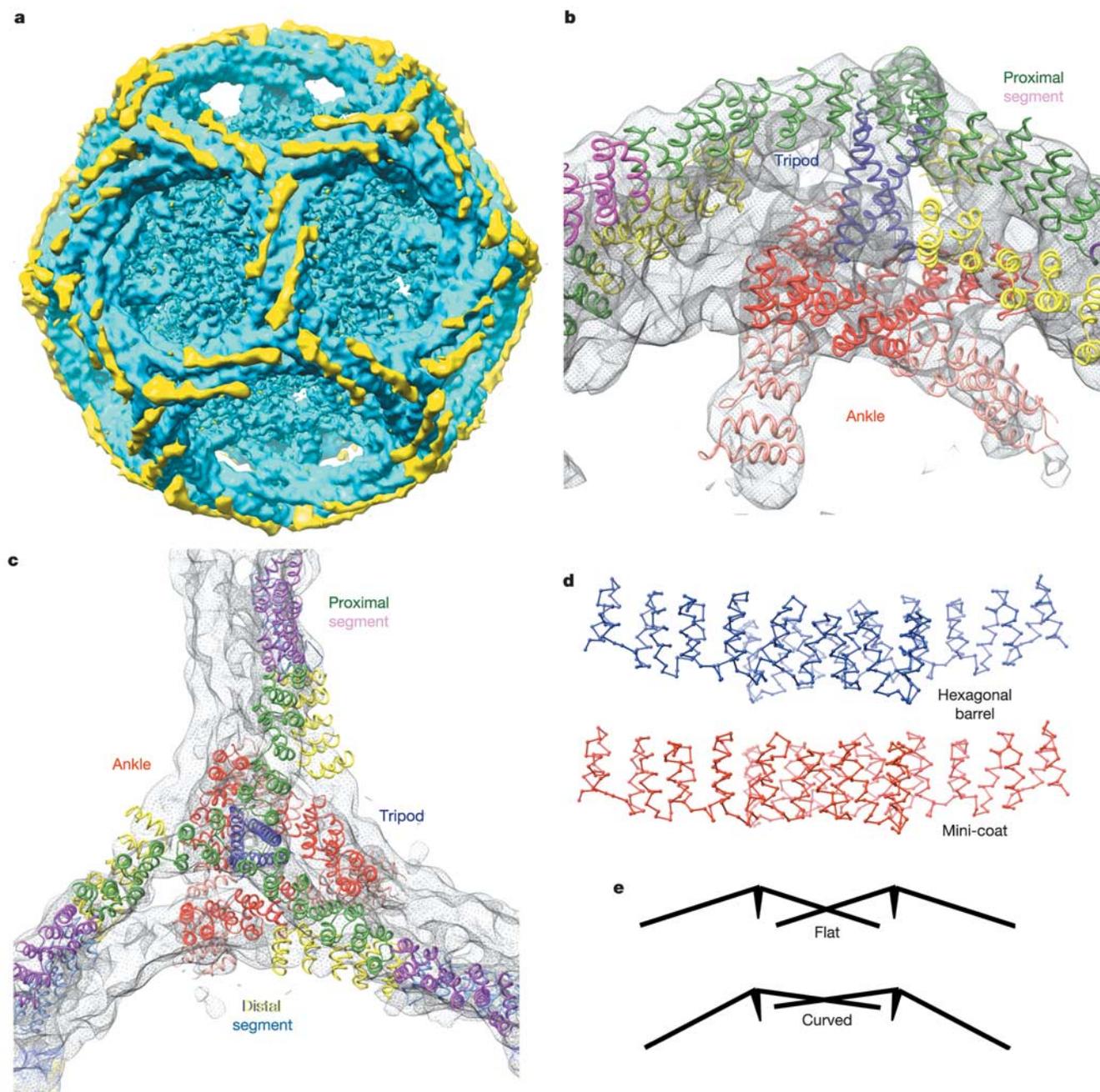


**Figure 7** How clathrin forms lattices with different curvature: the mini-coat. **a**, Image reconstruction of a tetrahedral coat at 13 Å resolution. The central density, from disordered AP-2 complexes, has not been flattened in this illustration, unlike Fig. 2. The light-chain difference density is in yellow; the density from light-chain-free coats is in blue. **b**, The hub assembly region, showing the fit of the proximal–distal pairs (green and yellow, respectively), ankle segments (salmon and red) and tripod (blue), transplanted directly from the model of the hexagonal-barrel coat, without adjusting relative orientations. Colours are those of the corresponding CHCR segment in Fig. 4a. **c**, A hub viewed from outside the coat, again with the directly transplanted model from the hexagonal barrel structure. Colour coding as in **b**. **d**, The crossing angles of two proximal segments in the edges of an hexagonal barrel (blue) and tetrahedral coat (red). The two differ by about 8°. **e**, Coats of different curvature can form from triskelions of constant pucker, by variation of the proximal-arm crossing angle. Projections of a pair of triskelions, with flat packing (upper) or curved packing (lower).

The functions of the clathrin light chains are still obscure. They appear to have no effect on assembly driven by adaptors (this work) or uncoating[24]. The location of the light chain on the outside of the cage is consistent with a role in communicating with cytoplasmic structures rather than in cargo-oriented regulation.

## Tetrahedral particles

Mini-coats were selected from the same micrographs used for the hexagonal-barrel image analysis just described. We used 920 particles of light-chain-free and 890 particles of light-chain-bound forms. Despite the small number of particles, the final tetrahedral symmetry averaged reconstructions (Fig. 7a) were reliably computed to resolutions of 13.2 Å for light-chain-free and 13.0 Å for light-chain-bound coats. There are seven symmetry-independent clathrin legs within a tetrahedral asymmetric unit, but we did not attempt further segmental averaging, as we did with D6 barrels. A mini-coat is about 620 Å in diameter, 80 Å smaller than a hexagonal barrel; its lattice is therefore more sharply curved. It nonetheless has the same overall organization and triskelion packing as seen in the hexagonal barrels (Fig. 7b, c). The light-chain map, computed as a difference between light-chain-bound and light-chain-free mini-coats (Fig. 7a), closely resembles the light-chain difference map for the barrels.

## Lattice adaptability

Clathrin can form structures of variable curvature, ranging from the small mini-coats to extended hexagonal arrays[4,25]. This adaptability is critical for function, as coated pits must engulf cargo of different shapes and sizes. Recent studies of clathrin dynamics illustrate that cargo diameter dictates the size (and hence the growth time) of a coated pit as it assembles at the plasma membrane[26]. We can imagine two distinct molecular mechanisms for achieving variable curvature with a single, trimeric assembly unit. In one, the anti-parallel contacts within an edge of the lattice remain essentially invariant, while the pucker at a triskelion vertex changes to fit the required local curvature. In the other, heavy-chain contacts within an edge vary, leaving the pucker constant while altering the crossing angle between antiparallel proximal–distal pairs (Fig. 7e). We have compared mini-coat and hexagonal-barrel coats, which have different lattice curvatures. If we extract from a hexagonal-barrel coat the model of an invariant hub, it fits with virtually no change in pucker into the hub density of a mini-coat (Fig. 7b, c). In other words, the difference in the curvatures of the two lattices resides in the crossing angles between proximal–distal pairs along the edges (Fig. 7d), not in changes in the organization of a vertex.

The curvatures of mini-coat and hexagonal-barrel lattices are only moderately different, and both are sharper than the average endocytic coated vesicle. Thus, we cannot rule out the possibility that in formation of extended, flat arrays, such as have been seen on the ventral surface of cells in culture and on endosomes, there will be additional points of flexibility. Some of the mini-coat hubs that embrace both pentagonal and hexagonal faces do have slight but detectable deviations from three-fold symmetry. We suggest, however (based on the total of 16 symmetry-distinct interactions we see in the barrel and mini-coats), that conservation of the proximal–distal contacts (which link triskelions centred on neighbouring vertices) and of the ankle brace (which links second-nearest neighbours) will be true of all specific clathrin assemblies.

The invariant contacts just described are primarily polar in character and restricted in extent. They are confined to the inner levels of the heavy-chain imbrications—just where we expect regulation by membrane-associated proteins to occur. In the accompanying paper[27], we show that auxilin, an important regulator involved in uncoating, associates with the hub assembly, where it could recruit the uncoating ATPase, Hsc70, to destabilize the ankle-brace contacts. □

## Methods

### Coat preparation, data collection and initial image processing

Coats were assembled[28], micrographs recorded, visually inspected on an optical diffractometer and only those showing clearly visible Thon rings[29] were digitized, particles picked, and initial reconstructions calculated as described in Supplementary Information. The first stages of image processing were performed using IMAGIC[30], resulting in a symmetry averaged three-dimensional reconstruction[31].

### Image refinement

Contrast transfer function (CTF) parameters were determined using CTFTILT[32]. Only micrographs for which CTF parameters could be determined accurately (fitting correlation coefficient $>0.20$) were selected. CTF parameters were calculated individually for each particle using values from CTFTILT (average defoci in two perpendicular directions, astigmatism angle at the micrograph centre, position of tilt axis and tilt angle) and $x$ and $y$ coordinates of the particle centre.

The three-dimensional model calculated from class averages was used as an initial reference for refinement by FREALIGN version 6.07 (ref. 33), which determines angular and shift parameters of the particles, corrects for CTF and computes a three-dimensional reconstruction. FREALIGN was run on a 30-node Linux cluster managed by LSF software (Platform Computing Corporation). Search and refinement of particle orientations were limited initially to a resolution range of 800–40 Å. A brute-force search (FREALIGN mode 3), with an angular step of 10°, was used to determine Euler angles and $x,y$ shifts of individual particles relative to the initial model. This search was followed by 10 cycles of iterative refinement. At this stage all particles were included in the three-dimensional reconstruction.

In subsequent refinement, we used only particles showing high cross-correlation with the reference (FREALIGN PRES $< 62°$, from 800 to 40 Å). Particle images were first re-cut from the original micrographs averaged over $3 \times 3$ pixels (pixel size, 4.2 Å; Nyquist limit, 8.4 Å). After 30 iterations, refinement in the 800–8.4 Å resolution range converged, as judged by stable PRES values. Particle images were then again re-cut from the original micrographs averaged over $2 \times 2$ pixels (pixel size, 2.8 Å; Nyquist limit, 5.6 Å). The final 10 refinement cycles were run on a 64-bit AMD Opteron workstation and included data in the 800–5.6 Å resolution range. Density in the centre of the three-dimensional reference model used for refinement was masked out using a soft-edged mask with a 40-pixel radius for $3 \times 3$ binned images and a 60-pixel radius for $2 \times 2$ binned images. At the end of the refinement process, a tight mask was applied to the three-dimensional reference model to flatten density corresponding to the surrounding solvent (FREALIGN XSTD parameter set to 2.0).

The nominal resolution of the final reconstruction was estimated from the spatial frequency at which the FSC fell to 0.143 (ref. 18). Reconstructed maps were low-pass filtered to exclude data beyond this resolution. A negative B-factor of 1,000 Å$^2$ was applied (in reciprocal space, as $\exp(-0.25Bs^2)$; $s$ is resolution in Å$^{-1}$) to the final reconstruction, to restore high-resolution contrast. The difference between light-chain-bound and light-chain-free coat densities was computed using a resolution bin-dependent scaling procedure implemented in EMAN[34]. Chimera[35] and O[36] were used to produce surface-rendered views of density.

### Local symmetry density averaging

Local symmetry EM density averaging used O[36] and MAVE[37] (Uppsala Software Factory). The atomic model of the proximal region[17] was placed into each of the local symmetry-related positions. A transformation from the reference position to each symmetry-related position was found with LSQ_EXPLICIT in O, using least-square minimization of distances between pairs of residues 1279, 1327 and 1516 in reference and rotated models. A 7.5-Å-radius mask was created around the atomic models. MAVE, which optimizes the real-space cross-correlation between the masked reference and symmetry-related density (command IMPROVE), was used to refine the operators, which were then used for local symmetry density averaging and for projecting the average onto a mask in the reference position (command AVERAGE). The averaged density was expanded onto masks in the rotated positions (command EXPAND). Density overlap from the expansion was removed using MAMA[38]. The FSC after n.c.s. averaging (Supplementary Fig. S1e) was computed by dividing the particles into two groups and calculating for each group an independent image reconstruction, which was then averaged (in segments) using the n.c.s. operators.

### Modelling atomic structures of clathrin fragments

Three-dimensional atomic structures of CHCR0-5 and CHCR7 were modelled (using MODELLER[39,40]) as described in the caption to Supplementary Fig. S3.

### Fitting atomic models into cryoEM maps

Clathrin atomic models were inserted into the local symmetry averaged clathrin coat EM density map using O[37]. The fit was optimized using rigid body refinement in MAVE (command IMPROVE). The reference electron density used for the optimization was calculated from the atomic model and filtered to the nominal resolution of the corresponding EM map using CCP4 programs SFALL and FFT[41]. Correlation coefficients of the fitting as output by MAVE ranged from 0.6 to 0.8. Positions of some of the terminal helices (helices $a$, $b$ and $i$, $j$) in the models for CHCR0–5 and CHCR7 were shifted to provide a better fit to density. Helical structures of the tripod and the light-chain fragment were modelled using Insight II (Accelrys).

1. Kirchhausen, T. Clathrin. *Annu. Rev. Biochem.* **69,** 699–727 (2000).
2. Robinson, M. S. Adaptable adaptors for coated vesicles. *Trends Cell Biol.* **14,** 167–174 (2004).

3. Brodsky, F. M., Chen, C. Y., Knuehl, C., Towler, M. C. & Wakeham, D. E. Biological basket weaving: formation and function of clathrin-coated vesicles. *Annu. Rev. Cell Dev. Biol.* **17,** 517–568 (2001).

4. Crowther, R. A., Finch, J. T. & Pearse, B. M. On the structure of coated vesicles. *J. Mol. Biol.* **103,** 785–798 (1976).

5. Kirchhausen, T. & Harrison, S. C. Protein organization in clathrin trimers. *Cell* **23,** 755–761 (1981).

6. Ungewickell, E. & Branton, D. Assembly units of clathrin coats. *Nature* **289,** 420–422 (1981).

7. Kirchhausen, T., Harrison, S. C. & Heuser, J. Configuration of clathrin trimers: Evidence from electron microscopy. *J. Ultrastruct. Mol. Struct. Res.* **94,** 199–208 (1986).

8. Ungewickell, E. Biochemical and immunological studies on clathrin light chains and their binding sites on clathrin triskelions. *EMBO J.* **8,** 1401–1408 (1983).

9. Kirchhausen, T., Harrison, S. C., Parham, P. & Brodsky, F. M. Location and distribution of the light chains in clathrin trimers. *Proc. Natl Acad. Sci. USA* **80,** 2481–2485 (1983).

10. Kirchhausen, T. *et al.* Clathrin light chains LCA and LCB are similar, polymorphic and share repeated heptad motifs. *Science* **236,** 320–324 (1987).

11. Jackson, A. P., Seow, H. F., Holmes, N., Drickamer, K. & Parham, P. Clathrin light chains contain brain-specific insertion sequences and a region of homology with intermediate filaments. *Nature* **326,** 154–159 (1987).

12. Vigers, G. P., Crowther, R. A. & Pearse, B. M. Three-dimensional structure of clathrin cages in ice. *EMBO J.* **5,** 529–534 (1986).

13. Vigers, G. P., Crowther, R. A. & Pearse, B. M. Location of the 100 kd-50 kd accessory proteins in clathrin coats. *EMBO J.* **5,** 2079–2085 (1986).

14. Smith, C. J., Grigorieff, N. & Pearse, B. M. Clathrin coats at 21 Å resolution: a cellular assembly designed to recycle multiple membrane receptors. *EMBO J.* **17,** 4943–4953 (1998).

15. Musacchio, A. *et al.* Functional organization of clathrin in coats: combining electron cryomicroscopy and X-ray crystallography. *Mol. Cell* **3,** 761–770 (1999).

16. Ter Haar, E., Musacchio, A., Harrison, S. C. & Kirchhausen, T. Atomic structure of clathrin—a β propeller terminal domain joins an α zigzag linker. *Cell* **95,** 563–573 (1998).

17. Ybe, J. A. *et al.* Clathrin self-assembly is mediated by a tandemly repeated superhelix. *Nature* **399,** 371–375 (1999).

18. Rosenthal, P. B. & Henderson, R. Optimal determination of particle orientation, absolute hand, and contrast loss in single-particle electron cryomicroscopy. *J. Mol. Biol.* **333,** 721–745 (2003).

19. Liu, S.-H., Wong, M. L., Craik, C. S. & Brodsky, F. M. Regulation of clathrin assembly and trimerization defined using recombinant triskelion hubs. *Cell* **83,** 257–267 (1995).

20. Kirchhausen, T. & Toyoda, T. Immunoelectron microscopic evidence for the extended conformation of light chains in clathrin trimers. *J. Biol. Chem.* **268,** 10268–10273 (1993).

21. Scarmato, P. & Kirchhausen, T. Analysis of clathrin light chain-heavy chain interactions using truncated mutants of rat liver light chain LCB3. *J. Biol. Chem.* **265,** 3661–3668 (1990).

22. Nathke, I. S. *et al.* Folding and trimerization of clathrin subunits at the triskelion hub. *Cell* **68,** 899–910 (1992).

23. Chen, C. Y. *et al.* Clathrin light and heavy chain interface: alpha-helix binding superhelix loops via critical tryptophans. *EMBO J.* **21,** 6072–6082 (2002).

24. Ungewickell, E. *et al.* Role of auxilin in uncoating clathrin-coated vesicles. *Nature* **378,** 632–635 (1995).

25. Heuser, J. Three-dimensional visualization of coated vesicle formation in fibroblasts. *J. Cell Biol.* **84,** 560–583 (1980).

26. Ehrlich, M. *et al.* Endocytosis by random initiation and stabilization of clathrin-coated pits. *Cell* **118,** 591–605 (2004).

27. Fotin, A. *et al.* Structure of an auxilin-bound clathrin coat and its implications for the mechanism of uncoating. *Nature* doi:10.1038/nature03078 (this issue).

28. Matsui, W. & Kirchhausen, T. Stabilization of clathrin coats by the core of the clathrin-associated protein complex AP-2. *Biochemistry* **29,** 10791–10798 (1990).

29. Thon, F. Zur Defokussierungsabhängigkeit des Phasenkontrastes bei der elektronenmikroskopischen Abbildung. *Z. Naturforsch.* **21a,** 476–478 (1966).

30. van Heel, M., Harauz, G., Orlova, E. V., Schmidt, R. & Schatz, M. A new generation of the IMAGIC image processing system. *J. Struct. Biol.* **116,** 17–24 (1996).

31. van Heel, M. *et al.* Single-particle electron cryo-microscopy: towards atomic resolution. *Q. Rev. Biophys.* **33,** 307–369 (2000).

32. Mindell, J. A. & Grigorieff, N. Accurate determination of local defocus and specimen tilt in electron microscopy. *J. Struct. Biol.* **142,** 334–347 (2003).

33. Grigorieff, N. Three-dimensional structure of bovine NADH:ubiquinone oxidoreductase (complex I) at 22 Å in ice. *J. Mol. Biol.* **277,** 1033–1046 (1998).

34. Ludtke, S. J., Baldwin, P. R. & Chiu, W. EMAN: semiautomated software for high-resolution single-particle reconstructions. *J. Struct. Biol.* **128,** 82–97 (1999).

35. Huang, C. C., Couch, G. S., Pettersen, E. F. & Ferrin, T. E. Chimera: an extensible molecular modeling application constructed using standard components. *Pacif. Symp. Biocomput.* **1,** 724 (1996).

36. Jones, T. A., Zou, J.-Y. & Cowan, S. W. Improved methods for building protein models in electron density maps and the location of errors in these models. *Acta Crystallogr. A* **47,** 110–119 (1991).

37. Jones, T. A. (ed.) *A, yaap, asap, @#*? A Set of Averaging Programs* (SERC Daresbury Laboratory, Warrington, 1992).

38. Kleywegt, G. J. & Jones, T. A. Software for handling macromolecular envelopes. *Acta Crystallogr. D* **55,** 941–944 (1999).

39. Marti-Renom, M. A. *et al.* Comparative protein structure modeling of genes and genomes. *Annu. Rev. Biophys. Biomol. Struct.* **29,** 291–325 (2000).

40. Sali, A. & Blundell, T. L. Comparative protein modelling by satisfaction of spatial restraints. *J. Mol. Biol.* **234,** 779–815 (1993).

41. Collaborative Computational Project. The CCP4 suite: programs for protein crystallography. *Acta Crystallogr.* **D50,** 760–763 (1994).